Enclosure 3

Westinghouse Response to NRC Observation 3-3
(Non-Proprietary)

January 2021

OBS 3-3

Demonstrate with supporting analyses and discussion that the thermal models discussed in the thermal chapter accurately model the thermal-related phenomena for steady-state storage and transient operations.

SAR Chapter 5 described both three-dimensional (3D) and two-dimensional (2D) FLUENT models that were used in the SAR thermal analyses and which are the basis for the reported Important-to-Safety (ITS) component temperatures. The thermal analyses considered the W37 canister and W21H canister in the W180 storage cask, the W37 canister and W21H canister in the W110 transfer cask, and various thermal transient analyses (e.g., vacuum drying).

a. It is noted in the thermal analysis that the PCT results for canister W37 (45 kW) and canister W21H (65 kW) were at similar temperatures. The chapter does not demonstrate how the unique thermal aspects associated with the W21H canister, with much greater power density (kW/m3), would have resulted in a similar PCT as the lower power density canister, nor does it provide input, convergence, energy balances, and solution values to confirm performance of the two canister models.

b. There was limited information and validation associated with the “equivalence” between the (transient) two-dimensional and three-dimensional thermal models, recognizing that a steady-state comparison between 2D and 3D models would not explicitly demonstrate appropriate consideration of thermal mass effects. Using appropriate models are needed to ensure bounding temperatures on important to safety components during steady-state and transient operations.

c. There was limited information on the methodology for modeling fin performance, in the 3D and 2D representations including fin effectiveness and fin efficiency found in ta detailed sub-model. It is noted that details of the turbulence model and its parameters would impact results, especially considering the flow field around the fins is within an enclosed annular gap; these details were not provided. Likewise, there was no validation of the “non-thermal equilibrium porous media” to model the 2D fins, which is an important heat transfer component.

Considering the extent of the above-mentioned issues that need to be addressed, the applicant can provide the input and output files of the 2D and 3D FLUENT thermal models presented in SAR Chapter 5 to aid the review.

This information is needed to determine compliance with 10 CFR 72.234(a) and 72.236(f).

Westinghouse Response:

Input and output files for the cases run using the three-dimensional and two-dimensional FLUENT thermal models will be made available for review by NRC in the SENTRY Reading Room.

a) The maximum Peak Cladding Temperature (PCT) of the W37 canister and the W21H canister (loaded in the W180 storage cask) are similar, even though their thermal powers are quite different. Factors influencing this observation are presented below:

- For both the W37 and the W21H canisters, the inputs and boundary conditions are the same for all of the cases. A detailed evaluation of the inputs and boundary conditions are presented below to confirm that they will not cause any differences between the maximum PCT for the W37 canister and for the W21H canister (loaded in the W180 storage cask) even though their thermal powers are quite different.

  - The environmental temperatures, insolation values, and external conditions (for example, percent of blockage in storage configuration or the presence of fluid in the cavity of canister and annulus of transfer cask condition during loading operations) for the SENTRY DSS in normal, off-normal, accident conditions and loading operations are discussed in Section 5.3 and defined in more detail in Sections 5.4.1.2 (for the storage configuration) and in Section 5.4.2.2 (for loading operations). The values used in the CFD models are listed in Table 5.4-1 and Table 5.4-19 of the SAR and are consistent between the two and three-dimensional model. It can be concluded that the inputs or boundary conditions will not lead to different PCT even though there are different thermal loads for the two canister designs.

  - System pressure inside the cavity for both the W37 and the W21H canister models is initially set to a value of [ ]$^{(a,c)}$ and is held constant for all steady-state and transient analyses. This pressure is the minimum guaranteed pressure from the helium backfill and therefore the adoption of this condition assures pressure is treated in a conservative manner as stated in Section 5.4.1.2. It can be concluded that the system pressure will not induce a change in the PCT between the two canister designs since both designs use the same system pressure.

  - In the thermal analysis of the SENTRY DSS, fuel assemblies are not explicitly modeled. Instead, fuel assemblies are approximated as rectangular parallelepiped porous media with internal heat generation. The porous media properties of thermal radial conductivity, thermal axial conductivity, specific heat, equivalent density, hydraulic loss, active fuel length and burnup profile have all been calculated to adequately represent thermally limiting fuel assemblies. All these properties are the same for W37 and W21H canisters and these properties (except for the radial conductivity) can be seen in Appendix 5A.1. The difference

between the radial conductivities of the two canisters is caused by the inherent characteristics of each design [ ]$^{(a,c)}$. This particular property will be evaluated in the follow section. It is discussed separately since it is the only porous media property that is different between the canister analyses.

- The design of W21H canister has been optimized to maximize heat rejection. The additional design features of the W21H canister contribute to the similar maximum PCT even though the thermal powers are so different. These design enhancements are discussed below:

  - The canister external temperature depends largely on the outer surface area of the canister, specifically the surface area available for heat transfer. The fins on the outer surface of the W21H canister significantly increase the available heat transfer area when compared to the available heat transfer area of the W37 canister. [

    ]$^{(a,c)}$ Considering only this parameter, the W21H canister would have a much lower temperature than the W37 canister.

  - Generically speaking, inside the canister, the temperature increases as the distance to the outer surface increases (for the same heat load). The outer diameter of the W21H canister [ ]$^{(a,c)}$ than that of the W37 canister (72 inches). Based only on this parameter, the W21H canister canister is able to accommodate a higher heat load while not increasing the calculated peak temperature.

  - The outer diameter of the W21H canister [ ]$^{(a,c)}$ than that of the W37 canister (72 inches). Generically speaking, this means that the heat path from the fuel assemblies to the ambient is shorter, producing a lower temperature gradient between the maximum temperature inside the canister and the exterior surface. This allows W21H canister to accommodate a higher heat load while not increasing the calculated peak temperature.

  - The loading patterns for W21H canister will always have an empty position in the center cell of the basket (see Section 5.4.1.1.2). For a completely loaded basket (all cells occupied with spent fuel), this center position will normally have the maximum temperature in the canister. By not loading the central cell, the W21H

temperatures do not peak in the center, but become more spread out even with a increased total heat load. Since the heat load distribution is more uniformly distributed and because there is one less SNF (20 SNF are loaded although there are 21 positions), the W21H canister is able to accommodate a higher heat load while not increasing the calculated peak temperature. Figure 1 shows the temperature distribution along the radius of the canisters in which this effect is seen.

- The W21H canister basket has been designed to maximize heat removal. The radial gap [ ]$^{(a,c)}$ was reduced to increase the thermal heat rejection via conduction (see Table 1 below). [ ]$^{(a,c)}$ Thus, these geometrical/material design features improve heat removal from the interior of the canister and this allows a higher heat load than the W37 canister.

Table 1 (Table 5.4-9 of SAR) – Basket-to-Shell Gaps in the Thermal Models

(a,c)

[ ]

(a,c)

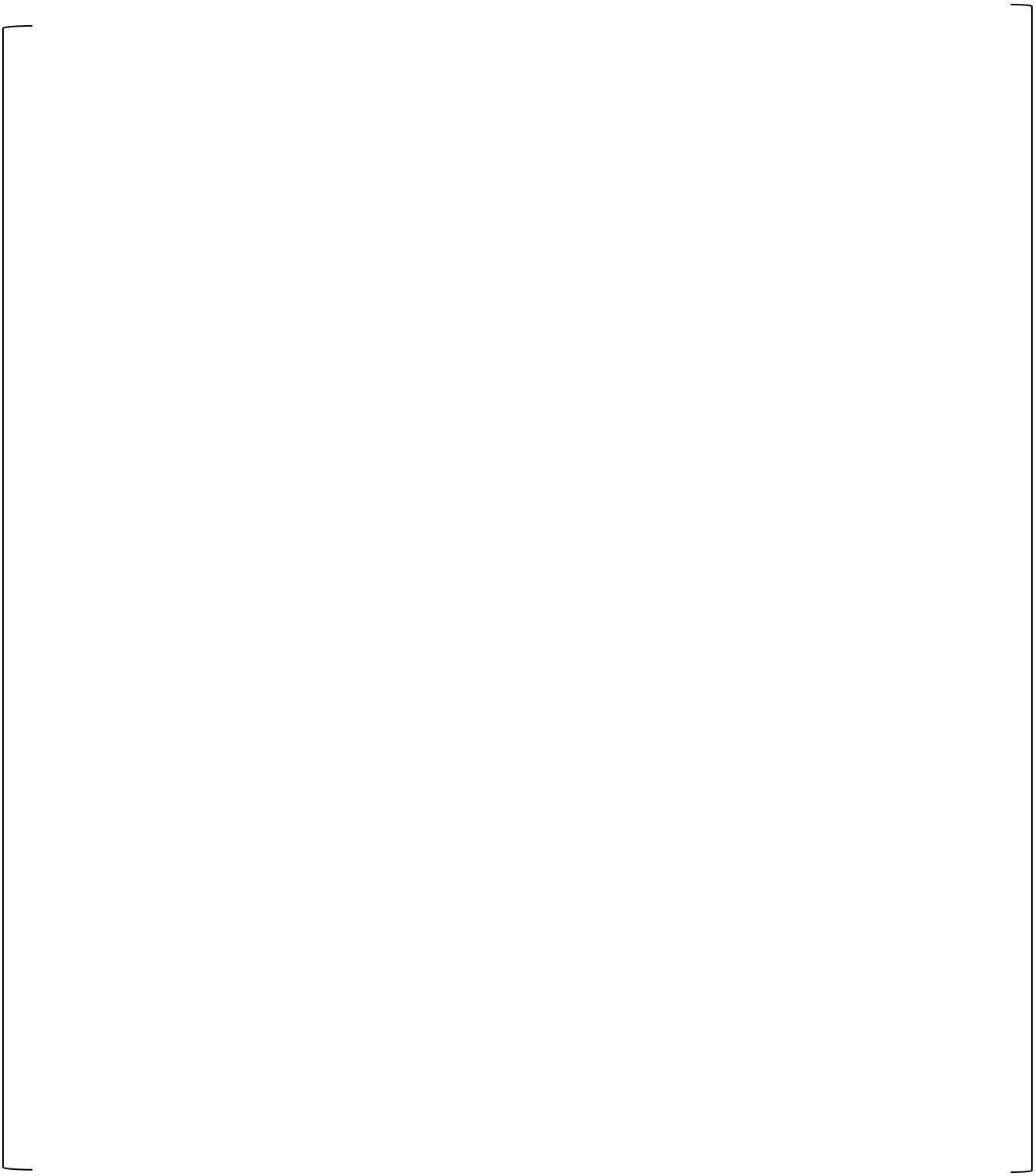

(a,c)

Taken together, these aforementioned results demonstrate a better thermal heat rejection for the W21H canister. Computationally, similar results for the W21H canister relative to the W37 canister were found even considering the higher relative thermal power in the W21H canister. The design features affecting the peak temperatures in the canisters are summarized and compared in Table 2.

Table 2 – Summary and Comparison of W37 and W21H Design Features

<table>
<tr><td>Canister</td><td>W37</td><td>W21H</td></tr>
<tr><td>Total Heat Load (kW)</td><td>45</td><td>65</td></tr>
<tr><td>Loading pattern
(Base Cases - Zonal Loading Pattern 1)</td><td> 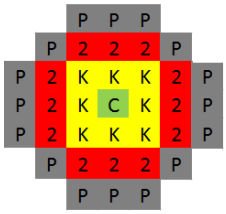

<table>
<tr><td>Zone</td><td>Heat per Position (kW)</td></tr>
<tr><td>P</td><td>1.22</td></tr>
<tr><td>2</td><td>1.42</td></tr>
<tr><td>C</td><td>0.5</td></tr>
<tr><td>K</td><td>1</td></tr>
</table></td><td> 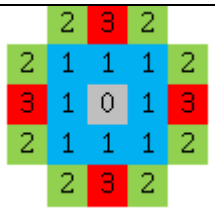

<table>
<tr><td>Zone</td><td>Heat per Position (kW)</td></tr>
<tr><td>1</td><td>2.350</td></tr>
<tr><td>2</td><td>4.325</td></tr>
<tr><td>3</td><td>2.900</td></tr>
<tr><td>0</td><td>0</td></tr>
</table></td></tr>
<tr><td>Basket plate thicknesses (inch)</td><td>Steel [ ]$^{(a,c)}$
Aluminum [ ]$^{(a,c)}$</td><td>Steel [ ]$^{(a,c)}$
Aluminum [ ]$^{(a,c)}$
MMC [ ]$^{(a,c)}$</td></tr>
<tr><td>Maximum hot basket-shell radial gap (inch)</td><td>0.14</td><td>[ ]$^{(a,c)}$</td></tr>
<tr><td>Aluminum emissivity (affects Fuel equivalent conductivity)</td><td>0.2</td><td>[ ]$^{(a,c)}$</td></tr>
<tr><td>External diameter (inch)</td><td>72</td><td>[ ]$^{(a,c)}$</td></tr>
<tr><td>External Area including fins (sqft)</td><td>295</td><td>[ ]$^{(a,c)}$</td></tr>
</table>

A balance of energy analysis for both canisters in their storage configuration for normal condition base case (Zonal Loading Pattern 1 for W37 and W21H) is now discussed to help understand the thermal behavior of SENTRY™ system.

Figure 3 shows the geometry of the cells and aluminum shape guides through which the mass of helium flows for the W37 canister. Table 3 shows the upwards helium mass flow rate in the fuel assemblies cells as well as the convective heat flux for the W37 canister while Table 4 shows the downward helium mass flow rate in the aluminum shape guides. These two tables show that the mass flow rate going up is equivalent to the mass flow rate going down. The convective heat flux is analyzed to determine the quantity of heat dissipated from the SNF by the coolant flow. All the values in these

tables (mass flows, inlet and outlet temperatures) have been extracted from the outputs of the Computational Fluid Dynamics (CFD) analysis. The only exception is the convective heat that which is calculated by a formula using the previous values. (a,c)

(a,c)

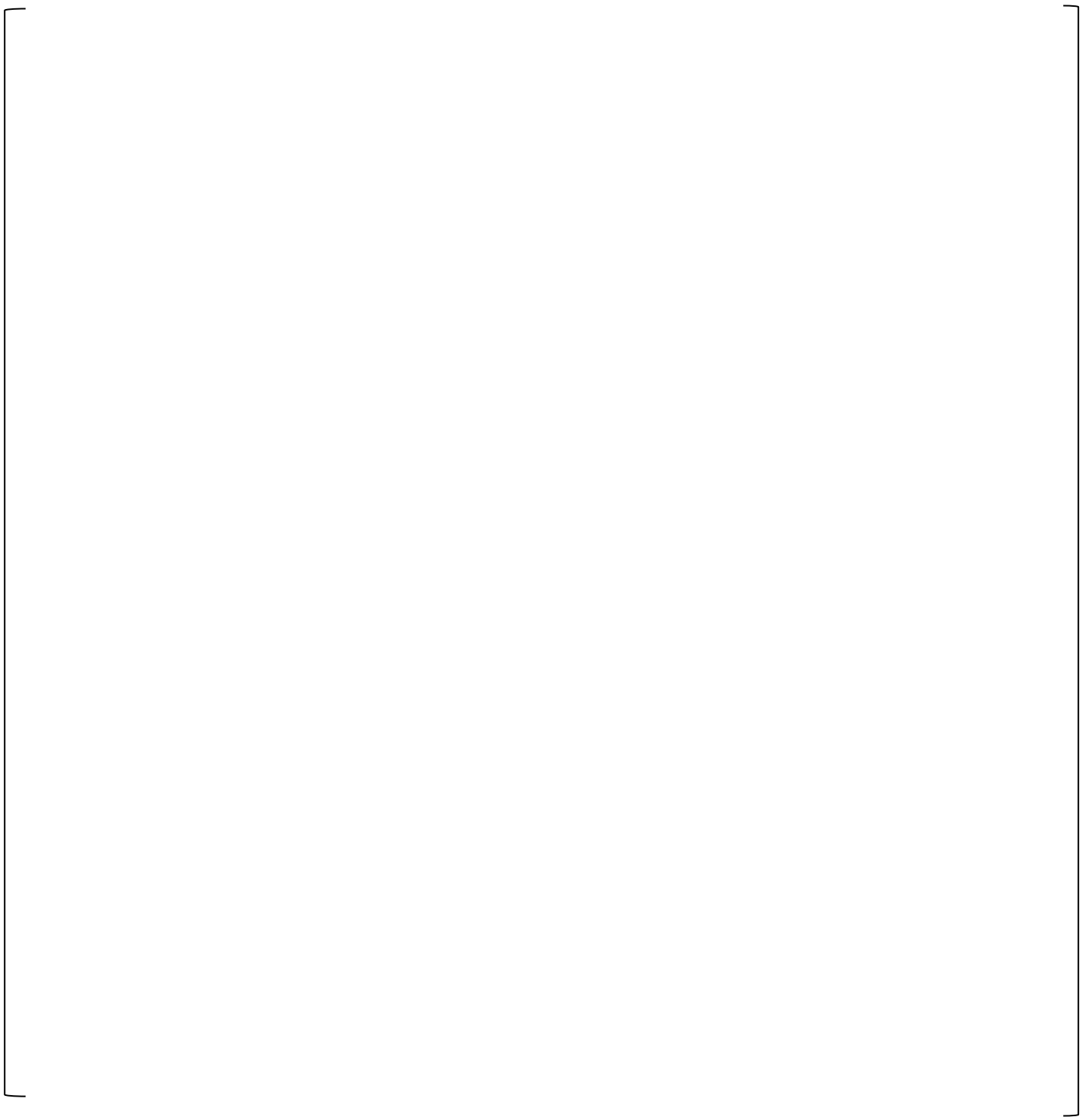

(a,c)

[

]

Except for a small portion of the heat that initially raises the fuel temperature, the heat generated in the SNF is transmitted outside the cells by internal convection, conduction and radiation. The relative fraction of energy transmitted by these mechanisms is presented in Table 7. While it is straightforward on how to obtain the amount of heat convected away, the calculation of the other two mechanism is an approximation as the interaction between the two mechanisms makes it very difficult to precisely quantify their individual contribution in the system.

However, Table 7 presents a good estimation of how the heat is transmitted away from the SNF. In both canisters, the effect of conduction and radiation has a larger contribution than convection. But, the fraction of energy transfer with conduction and radiation in the W21H canister is much larger than the fraction transmitted in the W37 canister. [

]$^{(a,c)}$ The effect of this optimization is evident in the results shown in Table 7.

Table 7 – W37 and W21H SNF Heat Transfer Mechanism Distribution

		Internal Heat Transfer Mechanism Distribution					
Canister	Total Heat (kW)	Convection		Cond. + Rad.		Total	
W37	45	19.44 kW	43%	25.56 kW	57%	45 kW	100%
W21H	65	15.84 kW	24%	49.16 kW	76%	65 kW	100%

Table 8 represents how the heat is dissipated in the external part of the canisters. The predominant mechanism is the natural convection in the annulus between the canister and the W180 storage cask as expected. The values for conduction, radiation and convection have been extracted from Fluent analysis. Closer examination on the fraction of heat transferred by convection (which is related to surface area) shows a significant increase in convective heat transfer for the W21H canister due to the design improvements when compared to the W37 canister.

Table 8 – W37 and W21H Heat Transfer Mechanism Distribution from the External Parts of the Canisters

Canister	W37		W21H	
	Heat (kW)	%	Heat (kW)	%
Conduction	2.7	6%	2.4	4%
Radiation	17.9	40%	10.6	16%
Convection	24.6	54%	52.0	80%
TOTAL	**45.2**[1]	**100%**	**65.0**	**100%**

Finally, the heat transfer distribution on the external portions of the W180 Storage Cask for W37 and W21H canisters is presented in Table 9. The main mechanism is again the internal convection in the annulus between canisters and the internal part of W180. Some of the inputs used to calculate the amount of convective heat transfer are presented in Table 10 with the values extracted from the appropriate Fluent analysis. The amount of insolation imposed on the external part of the W180 storage cask is also included in Table 9 for completeness in the heat balance since this mechanism provides additional heat to the system. The specific contributions from insolation are presented in Table 11.

[1] This value is extracted form Fluent and has a variability for the interaction in the heat fluxes.

Table 9 – Heat Transfer Distribution from the External Portions of the W180 Storage Cask

Canister	W37		W21H	
	Heat (kW)	%	Heat (kW)	%
Radiation	12.2	22%	11.5	16%
External Convection	6.9	13%	6.4	9%
Internal Convection	35.8	65%	56.1	76%
Insolation	-9.6	-	-9.6	-
	45.3	**100%**	**64.4[2]**	**100%**

Table 10 – Select Inputs used to Calculate Convective Heat Transfer to the Air Flow in the Annular Gap

	Air mass flow (kg/s)	T_{in} (K)	T_{out} (K)	Heat (kW)
W37	0.552	300.2	364.9	35.8
W21H	0.533	300.4	405.3	56.1

Table 11 – Insolation Heat in W180 Storage Cask

Surface	1/8 Surface Area (FLUENT)	Entire Surface Area (m^2)	q at 12 hours (W/m^2)	q at 24 hours (W/m^2)	absorptivity	Q (W)
Lateral – Steel	0.0375	0.30	400	200	0.3	18
Lateral - Concrete	8.0441	64.35	400	200	0.65	8365
Upper part - Steel	1.3133	10.51	800	400	0.3	1260
					Q Insolation	9645

[2] This value is extracted from Fluent and it has a variability as can be seen in Figure 22. This result is from the last iteration.

The computations (residuals) in the different Structures, Systems and Components (SSCs) were monitored throughout the code execution to insure convergence. Since natural convection is a transient process by nature, some variability in the residuals is to be expected. The monitored values are the maximum temperatures for each SSC. Figure 5 to Figure 11 show the results for the SSC using the W37 canister in W180 storage cask base case (zonal loading pattern 1 with DBF1). Figure 12 to Figure 19 show the results for the SSC using the W21H canister in W180 storage cask base case (zonal loading pattern 1 with DBF1).

All the values reported have a small temperature fluctuations with the exception of the canister temperatures. In this component, the turbulent flow of the helium below the area in which the maximum temperatures for the canisters are obtained induce some natural variability in the calculated results. Figure 20 gives some indications of the vortexes generated by the helium in the area of interest. However, even these fluctuations are not extreme, and the results show an adequate, engineering level of convergence.

Figure 5 – PCT in the W37 Canister

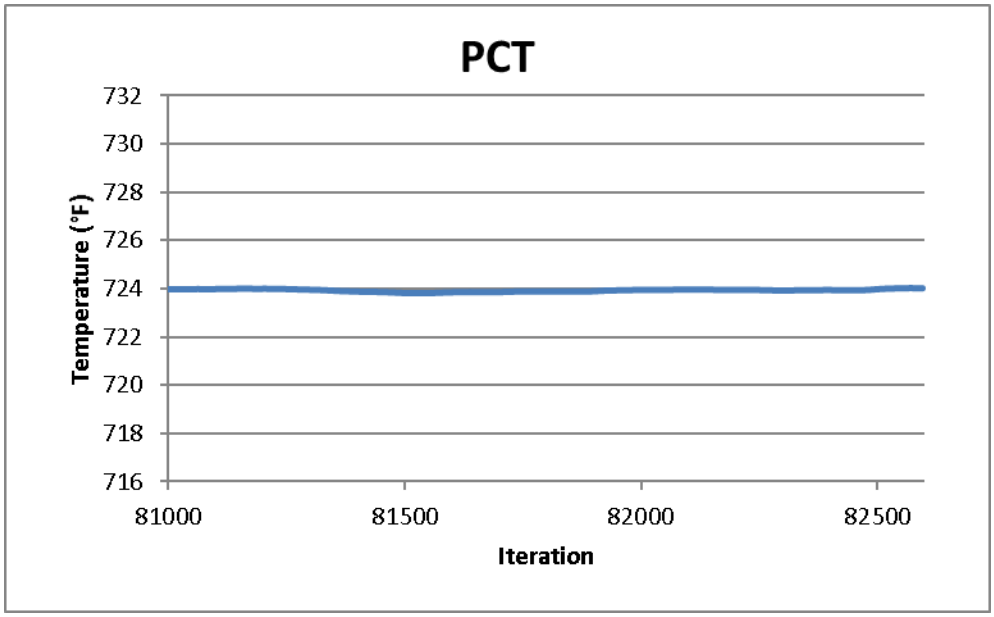

Figure 6 – Canister Temperature in the W37 Canister

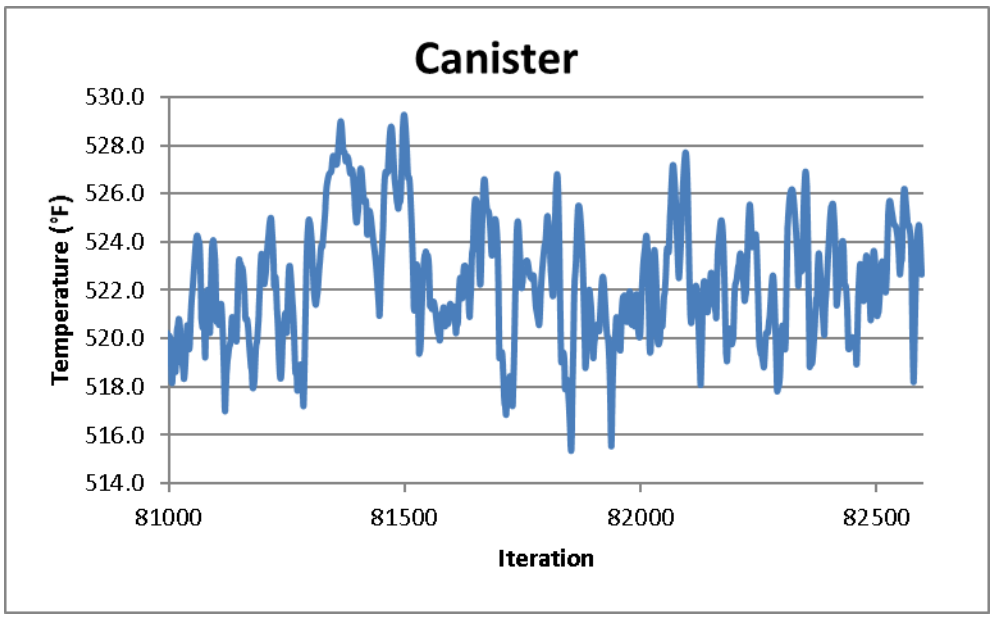

Figure 7 – Stainless Steel Basket Plate Temperature in the W37 Canister

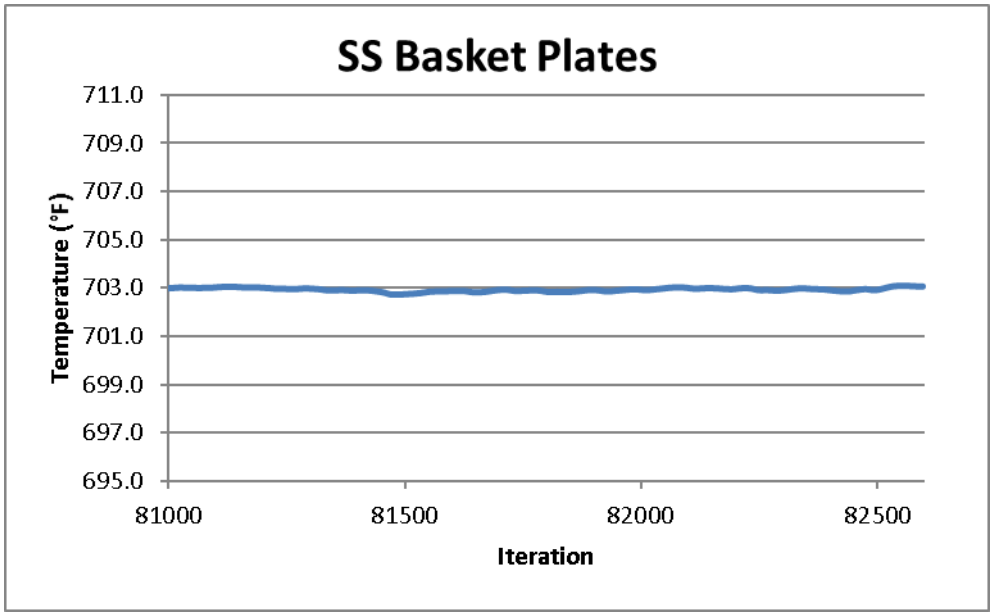

Figure 8 – Aluminum Basket Plate Temperature in the W37 Canister

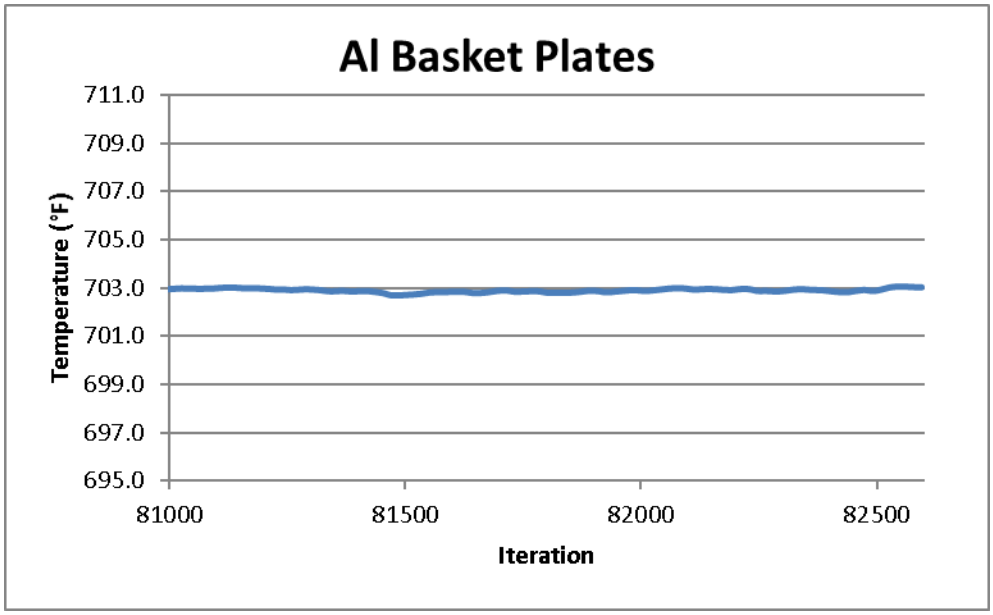

Figure 9 – Aluminum Basket Profile Temperature in the W37 Canister

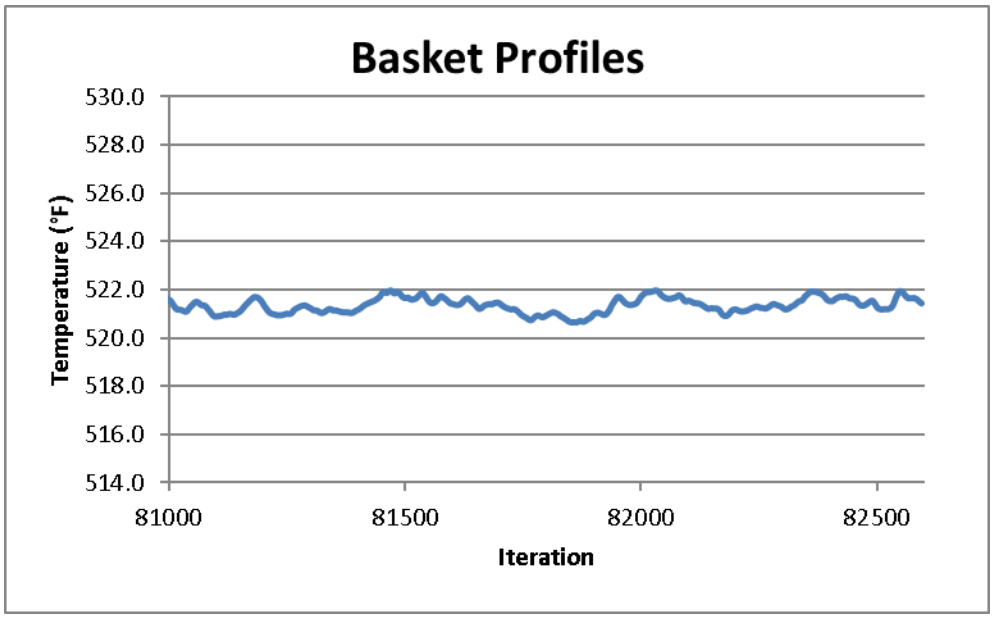

Figure 10 – Storage Cask Concrete Temperature in the W37 Canister

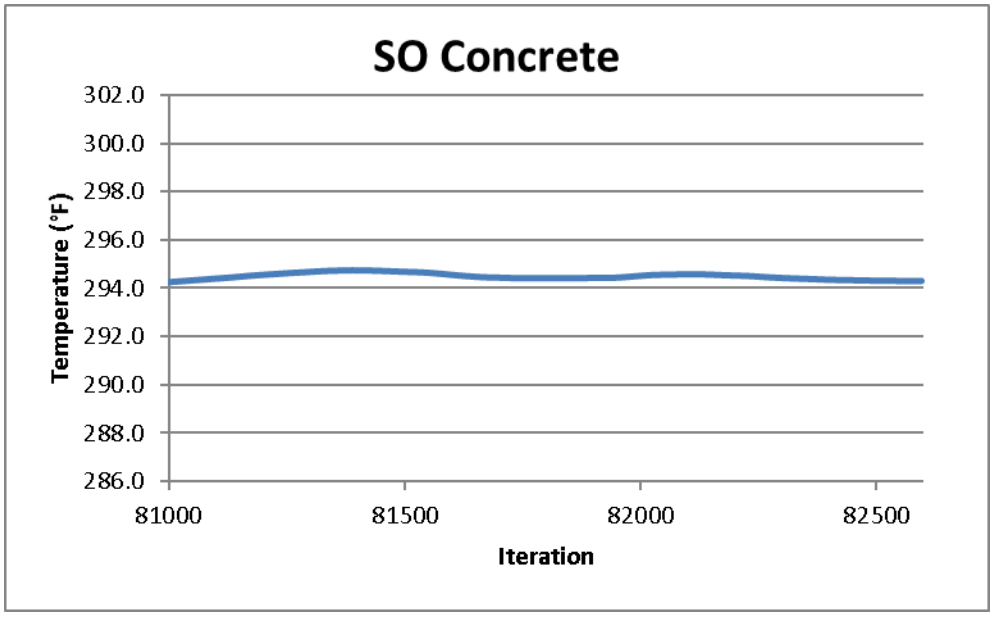

Figure 11 – Storage Cask Steel Plate Temperature in the W37 Canister

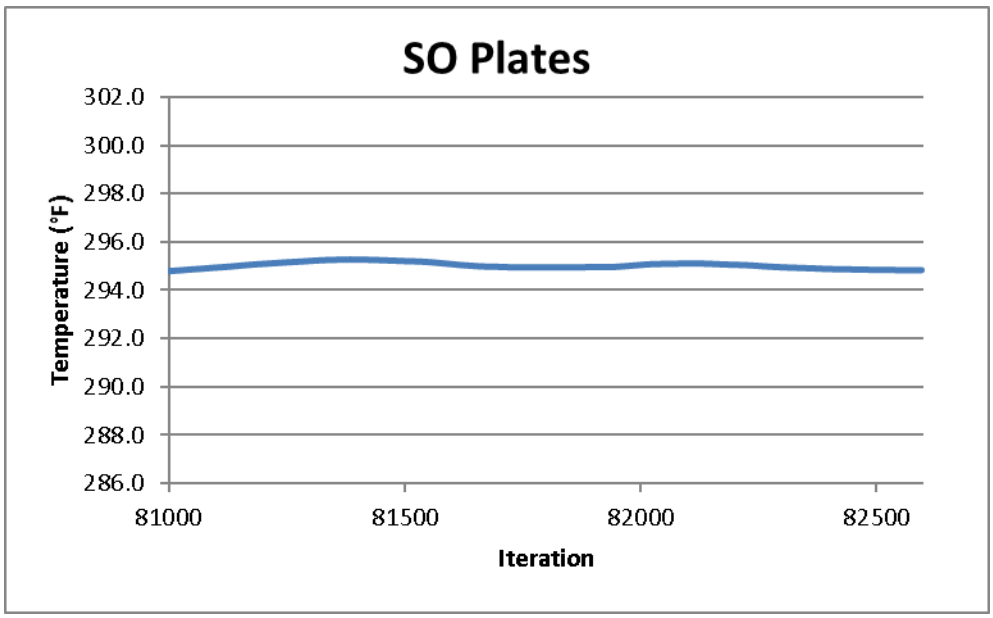

Figure 12 –PCT in the W21H Canister

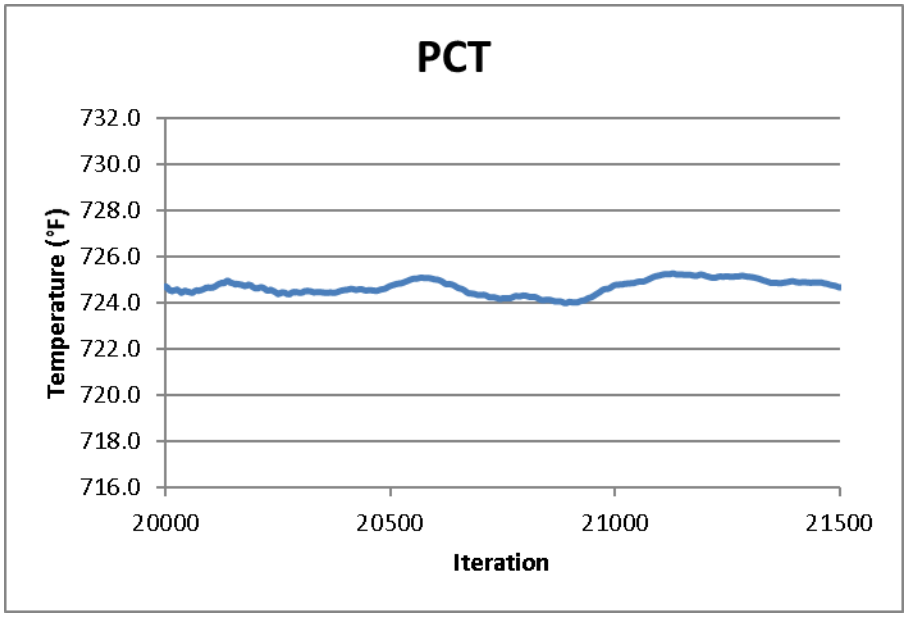

Figure 13 – Canister Temperature in the W21H Canister

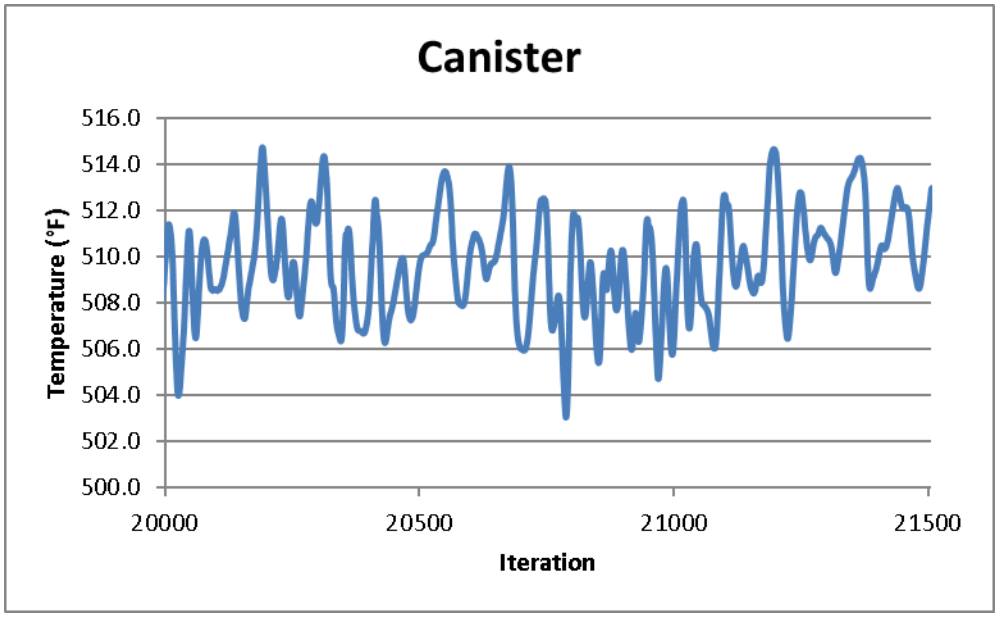

Figure 14 – Stainless Steel Basket Plate Temperature in the W21H Canister

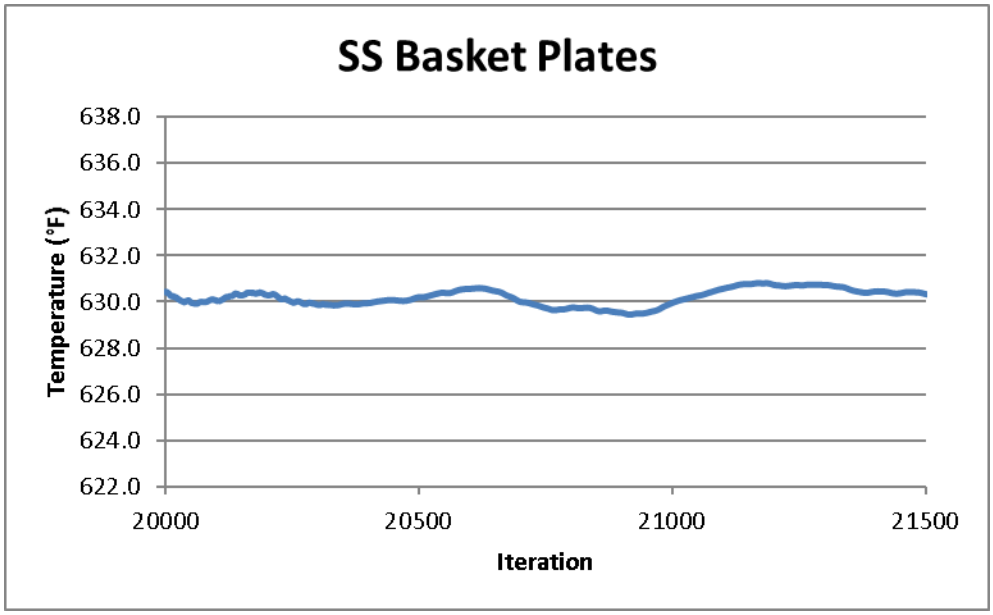

Figure 15 – Aluminum Basket Plate Temperature in the W21H Canister

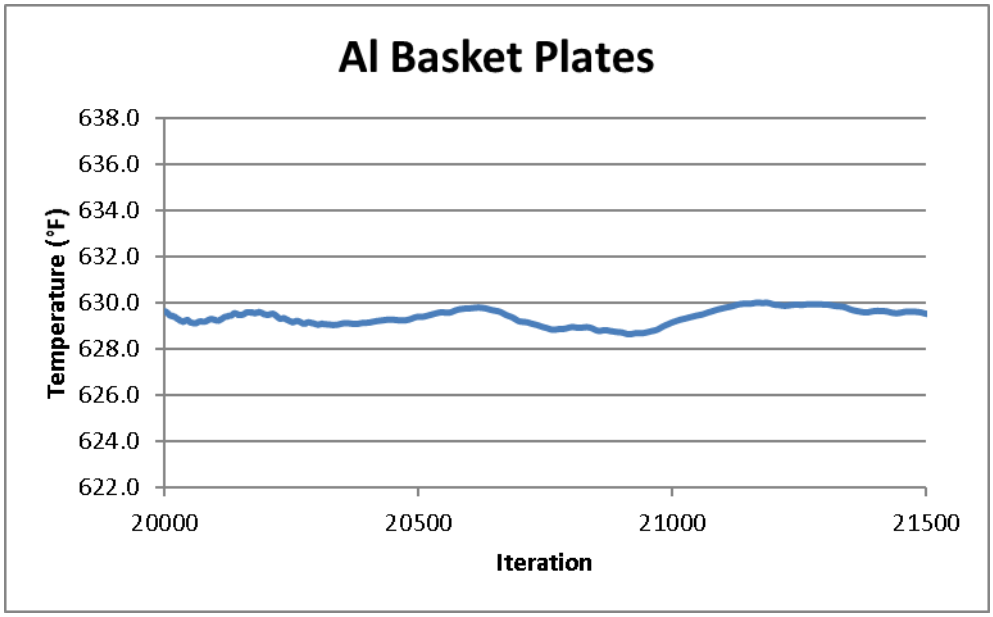

Figure 16 – MMC Basket Plate Temperature in the W21H Canister

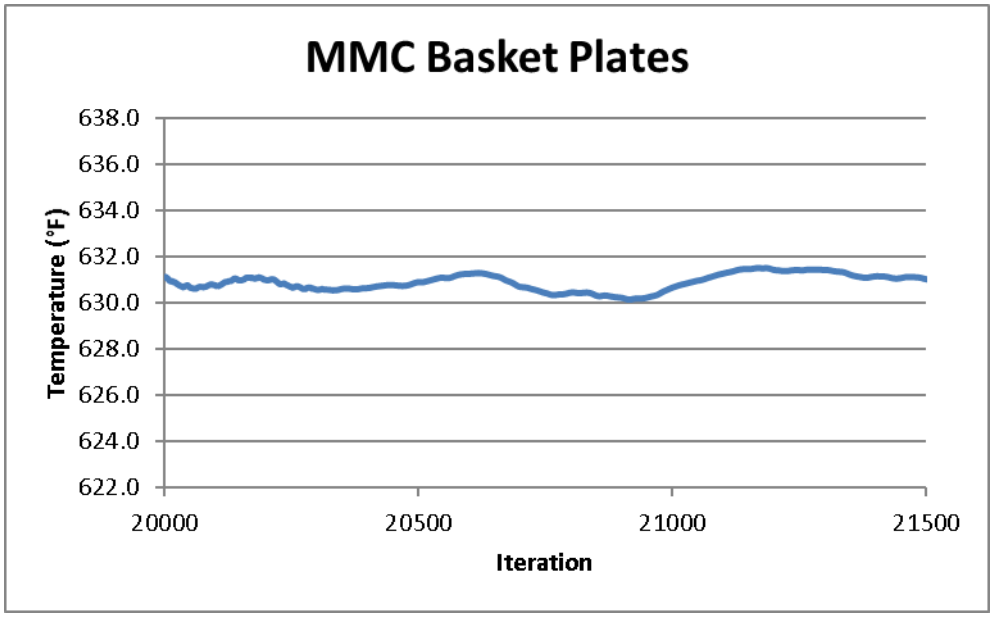

Figure 17 – Basket Profile Temperature in the W21H Canister

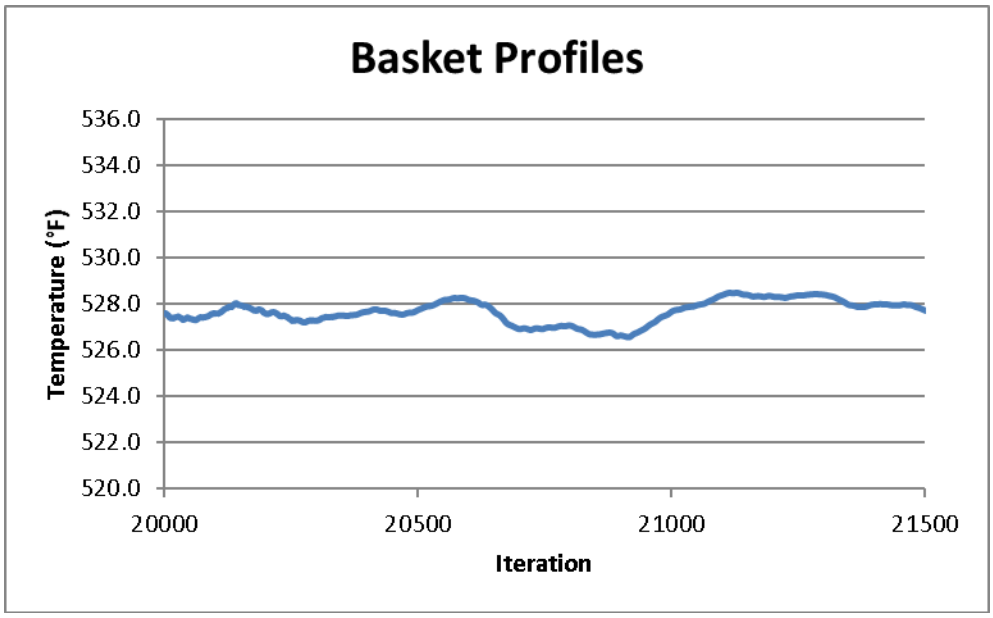

Figure 18 – Storage Cask Concrete Temperature in the W21H Canister

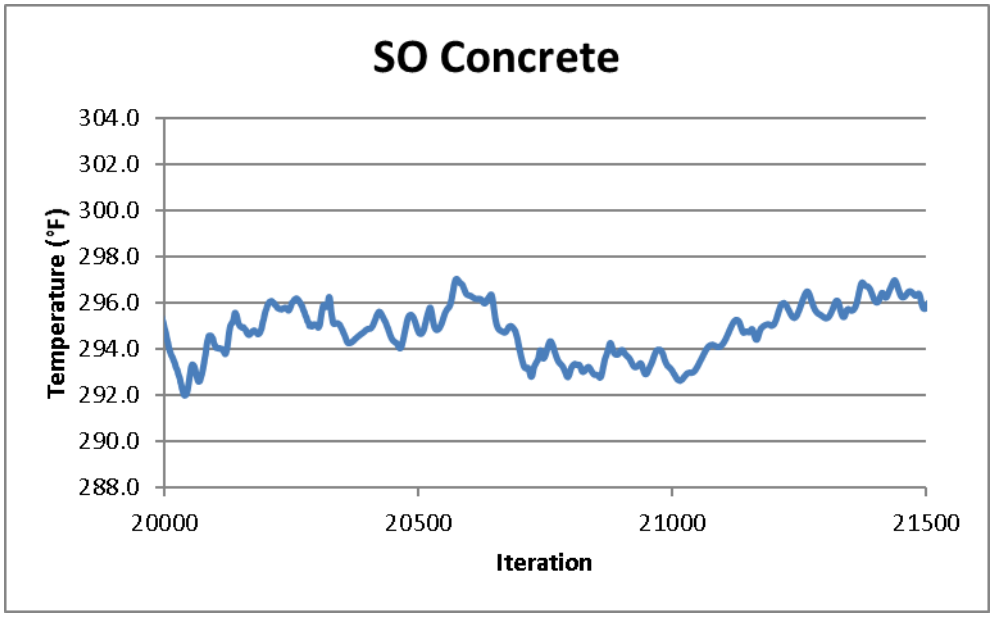

Figure 19 – Storage Cask Steel Temperature in the W21H Canister

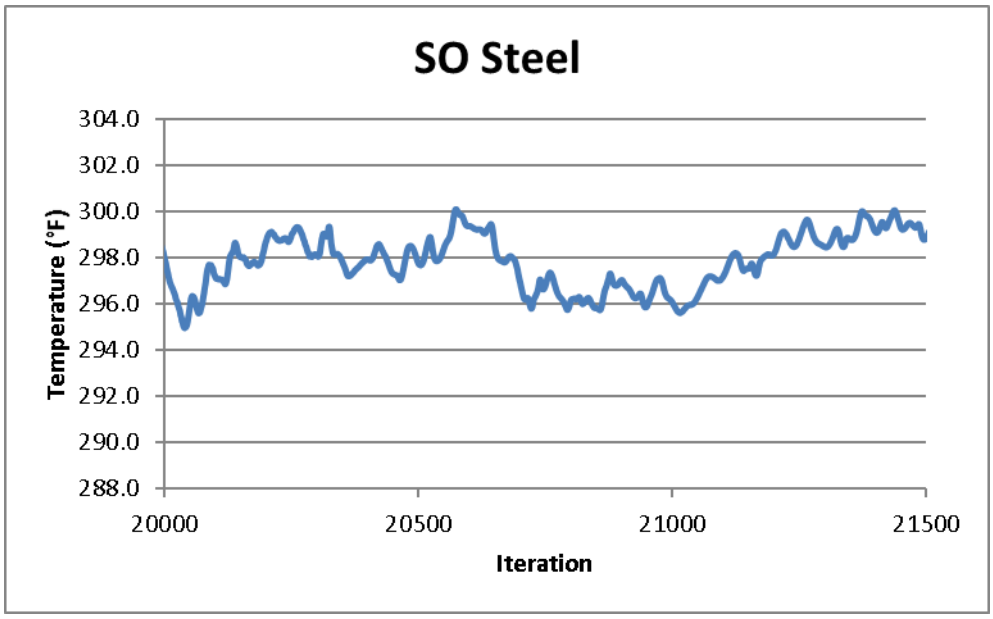

Figure 20 – W37 Canister Helium Flow in the Area below the Lid (a,c)

The CFD models have been run until they converged. This means that the solution no longer varies with additional iterations (as shown in the previous figures for the SSC) and that the residuals are below a prescribed root mean square (RMS) level (10^{-3} for continuity equations and 10^{-6} for energy equations). In reality, as stated in NUREG/CR-7260, "*some solutions are better behaved than others. … Some solutions are much "noisier," and their solution can vary significantly within a range of values.*" In the SENTRY system is identified a variation "*due to physically based unsteady flow patterns in the steady-state simulation*" as shown in Figure 20. Also, the vorticity in the inlet vent have an impact on the residuals. With the high resolution of the grid used for this analysis (as required by the SST k-w approach), the model captures very well the unsteady behavior at the vent inlet. This unsteady behavior makes it more challenging

to meet the convergence criteria. The residuals for the base case using the W37 and W21H canisters are shown in Figure 21 and Figure 22, respectively.

Figure 21 – Residuals from the W37 Canister Model in W180 Storage Cask (Base Case)

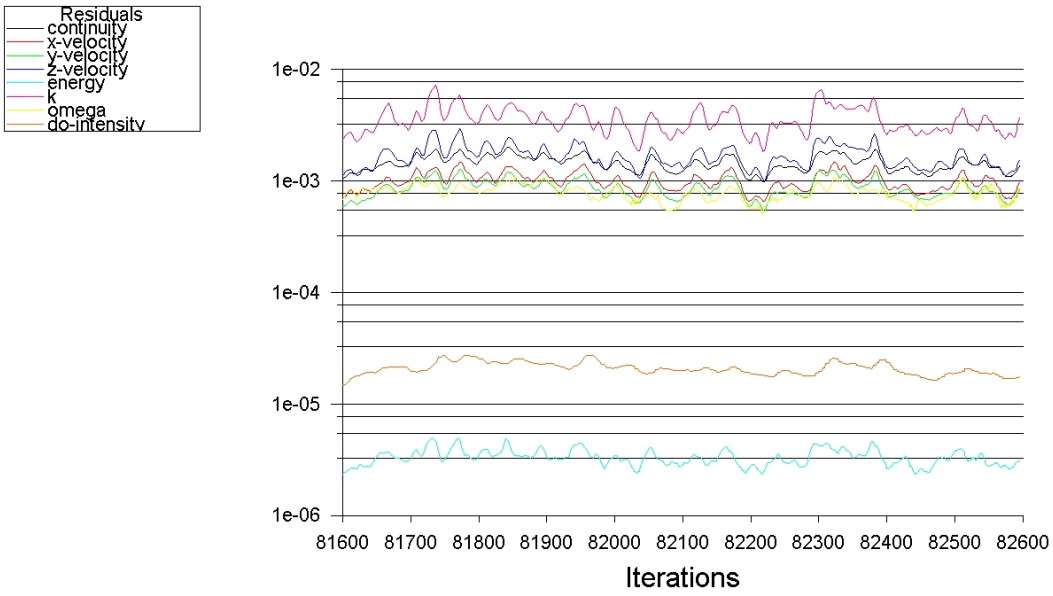

Figure 22 – Residuals from the W21H Model in W180 Storage Cask (Base Case)

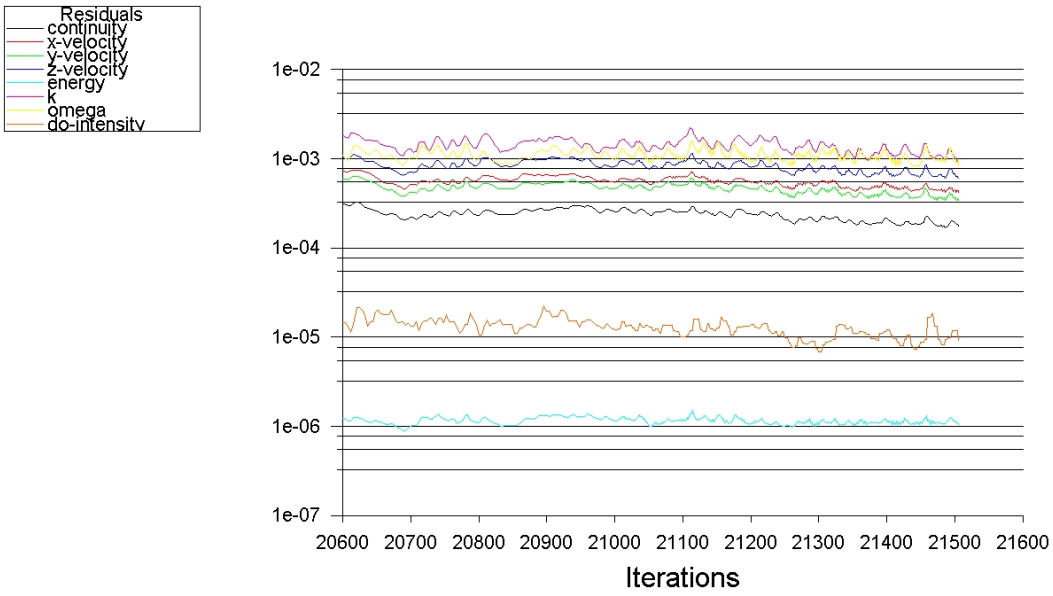

Other parameters of interest that were checked for convergence are the external heat flux in the outer part of the W180 storage cask (Figure 23 using the W37 canister and Figure 24 using the W21H canister), the cell helium flows (Figure 25 and Figure 26), and the storage cask air flow (Figure 27 and Figure 28).

Figure 23 – W37 Canister in the W180 Storage Cask – Outer Surface Heat Flux

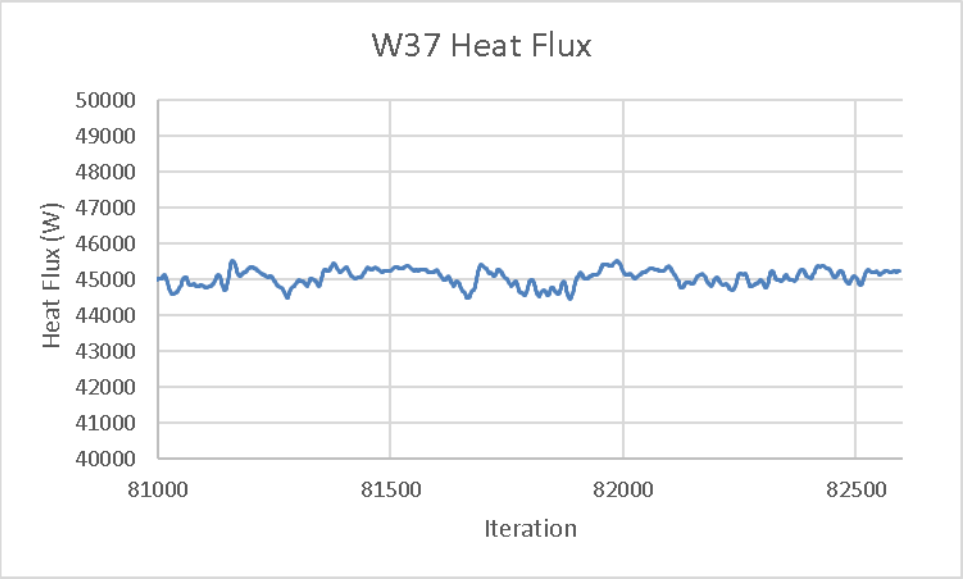

Figure 24 – W21H Canister in the W180 Storage Cask – Outer Surface Heat Flux

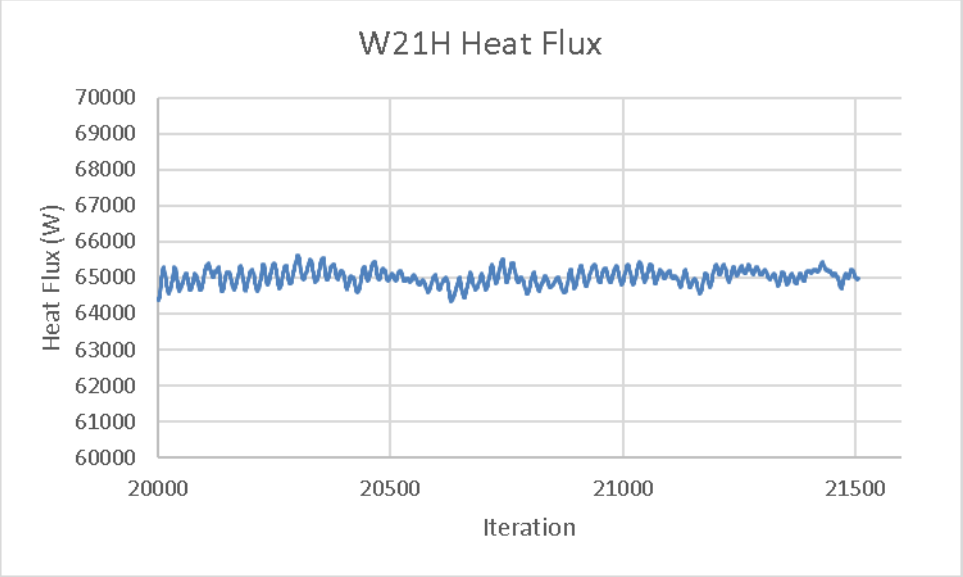

(a,c)

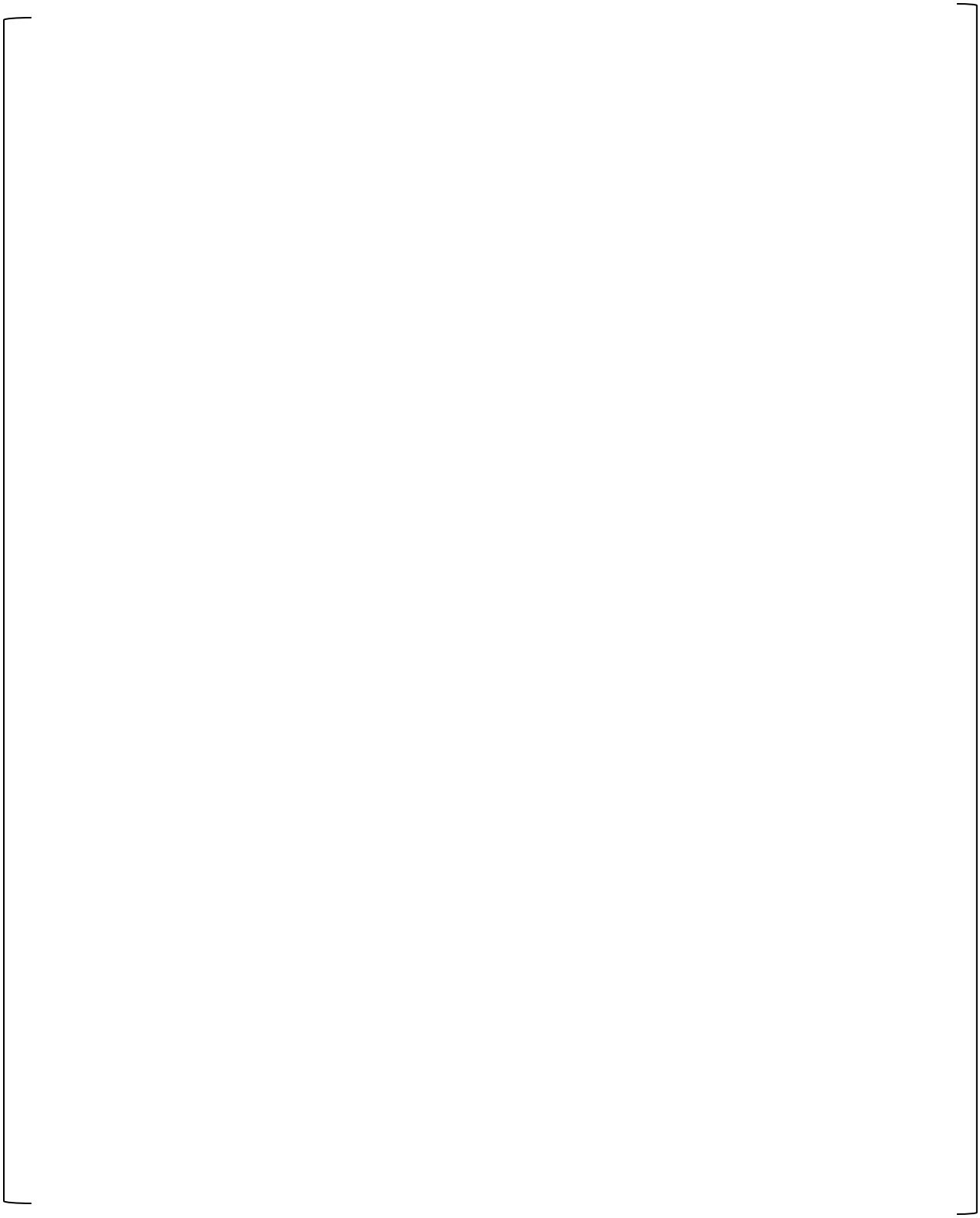

Figure 27 – Storage Cask Air Mass Flow Rate for the W37 Canister in the W180 Storage Cask

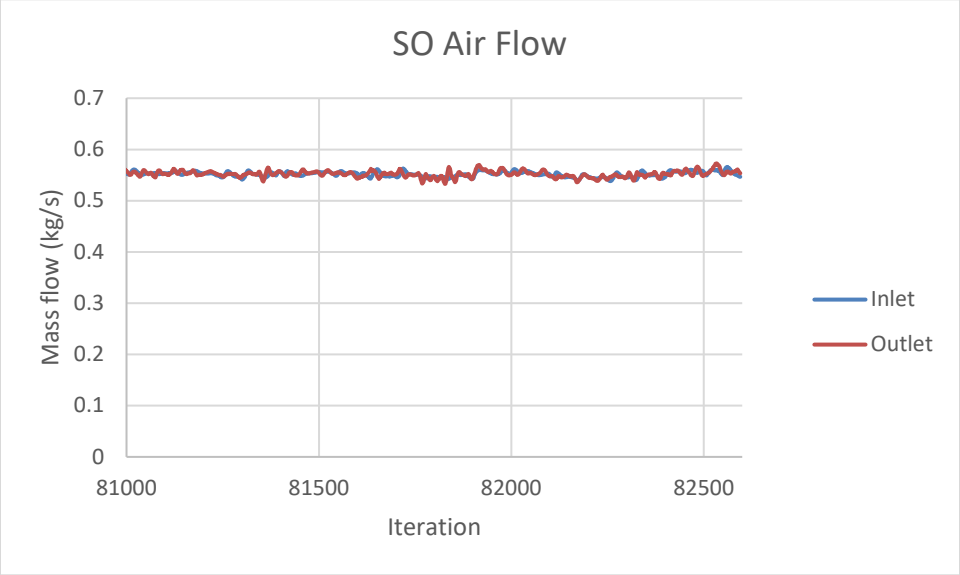

Figure 28 – Storage Cask Air Mass Flow Rate for the W21H Canister in the W180 Storage Cask

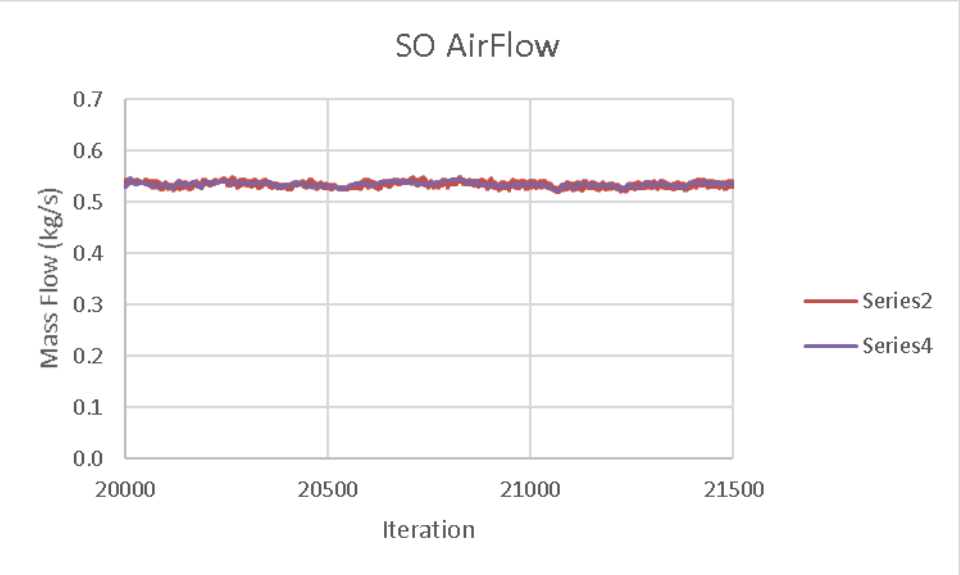

b) The validation and conservatisms of the two-dimensional models used to perform the loading operations analyses and fire and total blockage cases of accident analyses are shown in Chapter 5, Section 5A.2. [

]$^{(a,c)}$

[

]$^{(a,c)}$

(a,c)

(a,c)

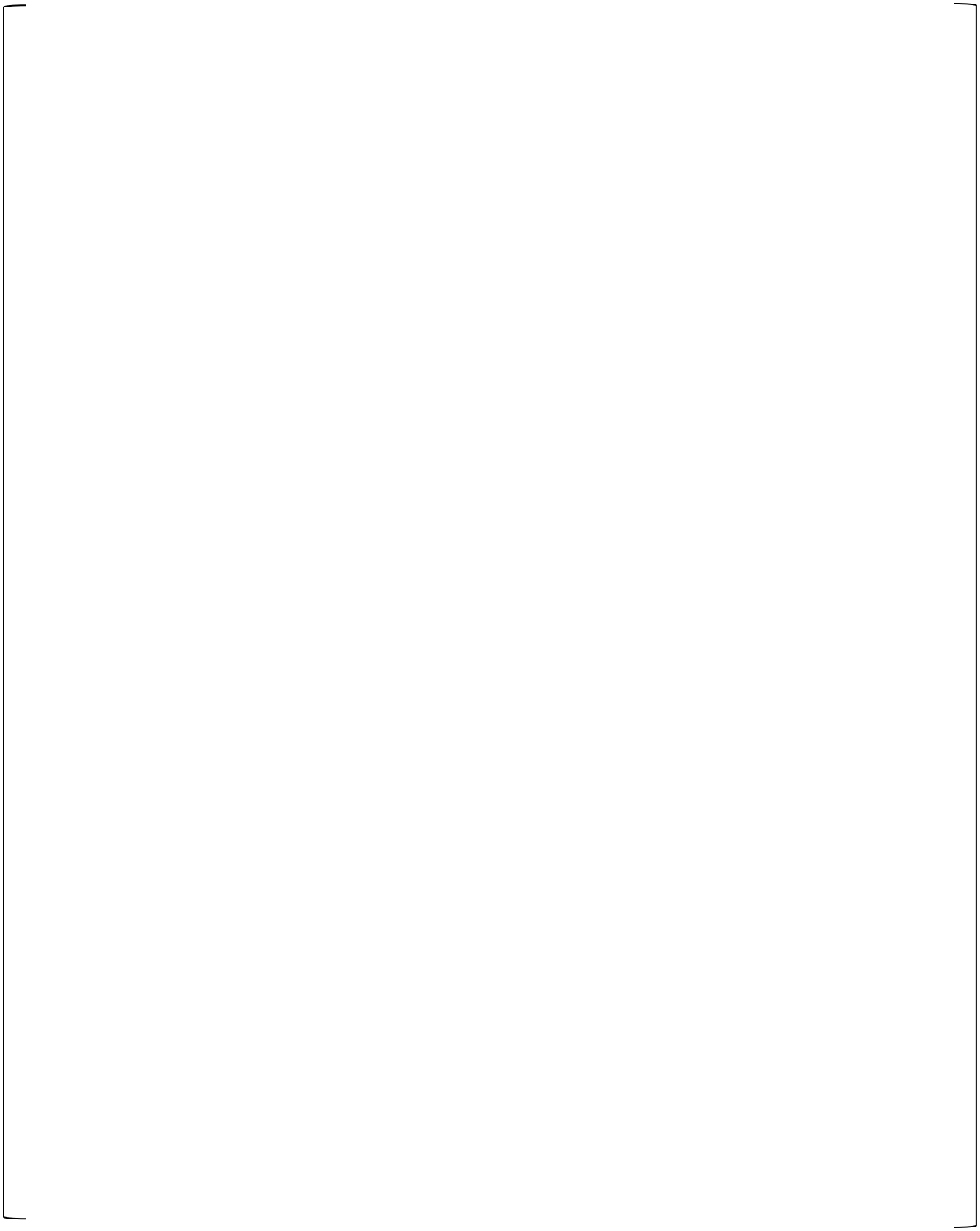

(a,c)

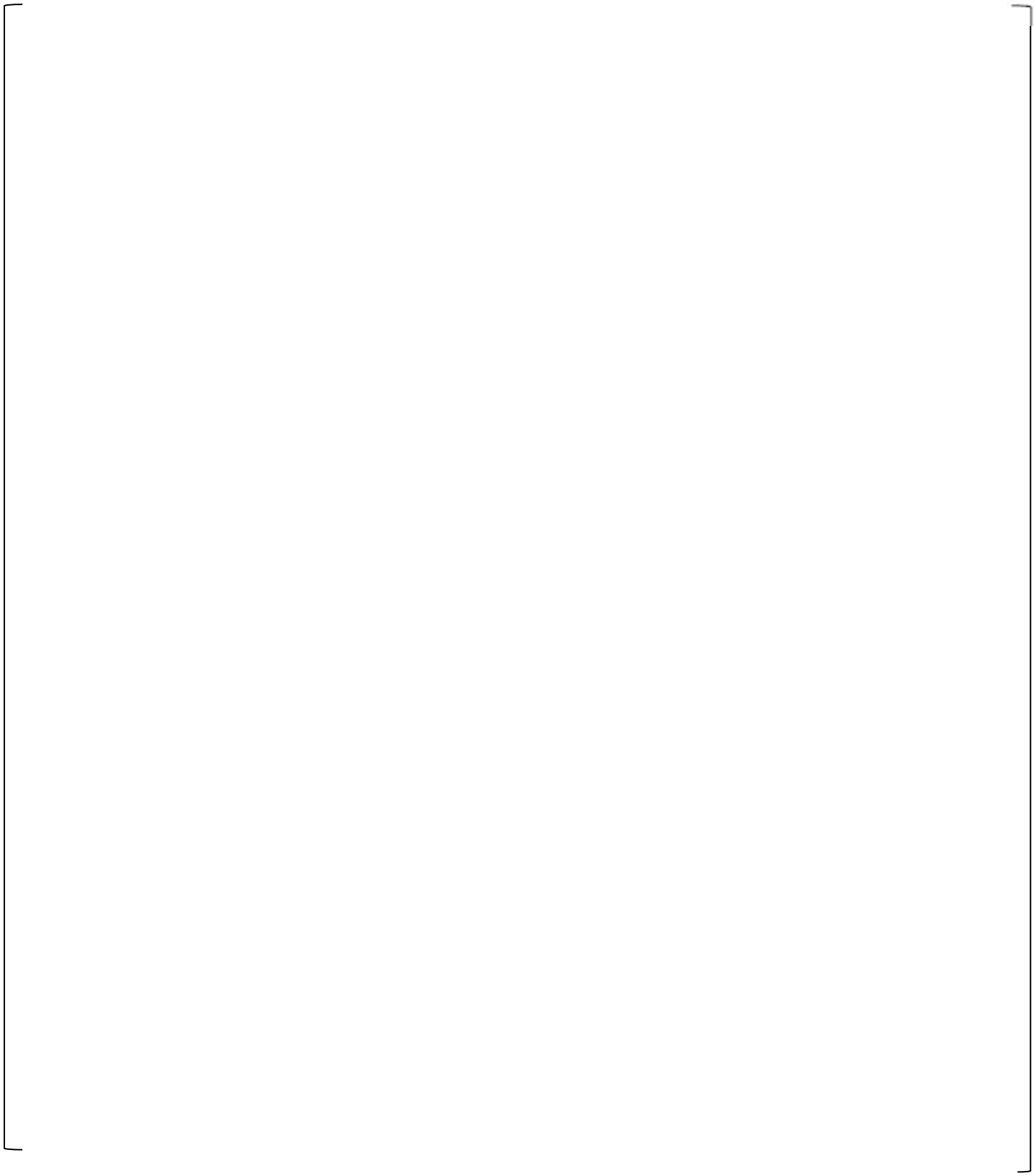

Figure 29 - Temperature Distribution along Radius from the 2D and 3D Results. Wet Phase for W37 canister

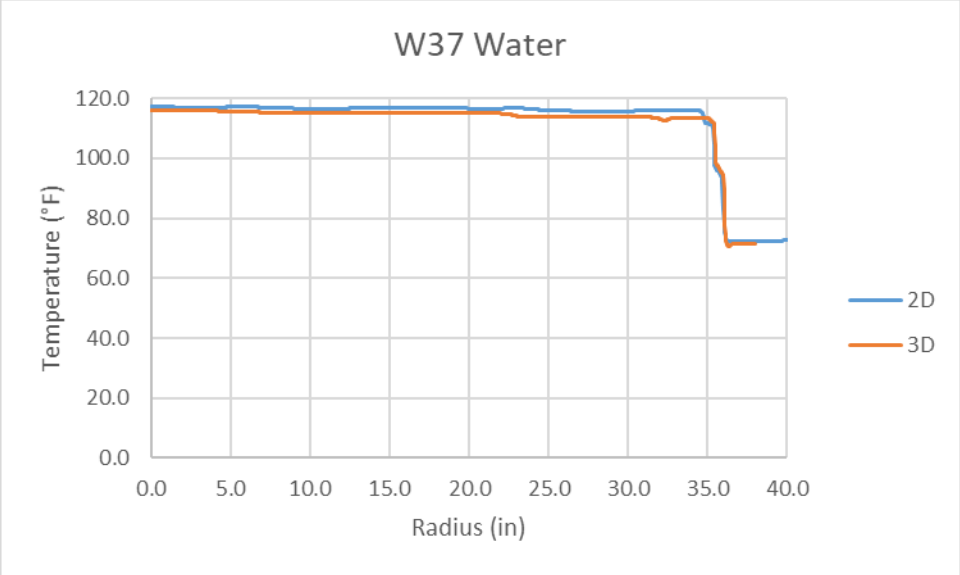

Figure 30 - Temperature Distribution along Radius from the 2D and 3D Results. Wet Phase for W21H canister

(a,c)

[

]

Figure 31 - Temperature Distribution along Radius from the 2D and 3D Results. Vacuum Phase W37 canister

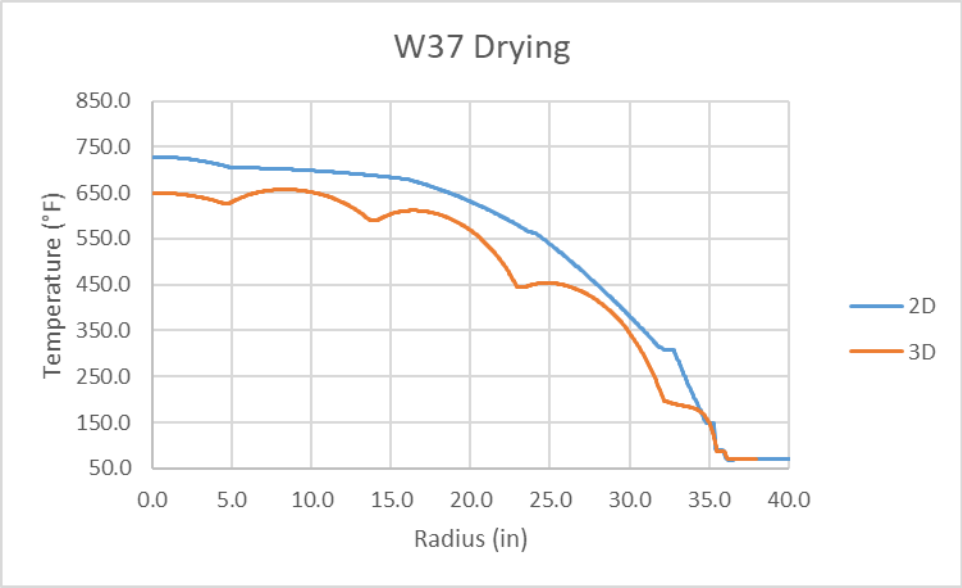

Figure 32 Temperature Distribution along Radius from the 2D and 3D Results. Vacuum Phase W21H canister (a,c)

[

]

Figure 33 - Temperature Distribution along Radius from the 2D and 3D Results. Helium Backfilled Phase W37 canister

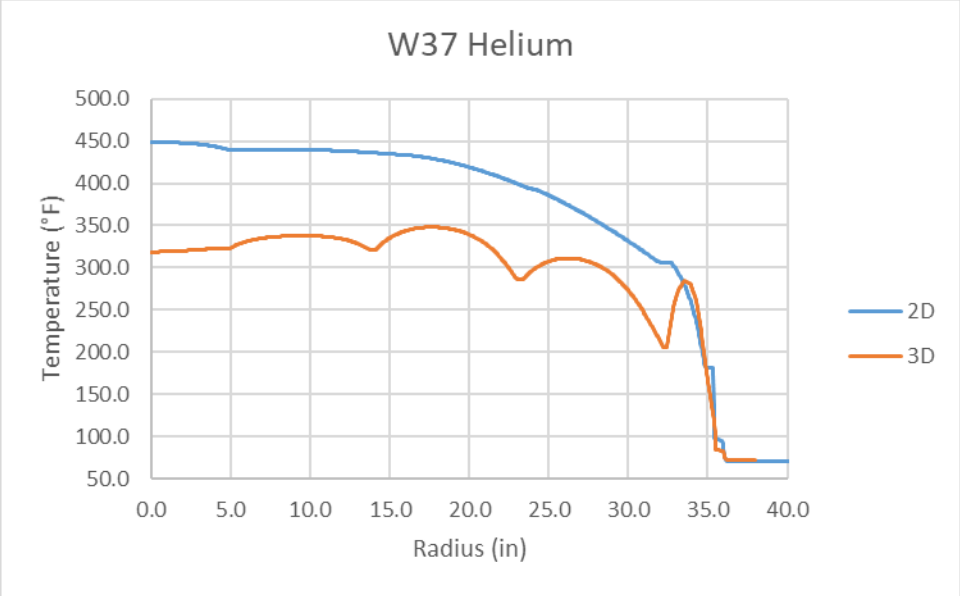

Figure 34 - Temperature Distribution along Radius from the 2D and 3D Results. Helium Backfilled Phase W21H canister

(a,c)

Figure 35 - Temperature Distribution along Radius from the 2D and 3D Results. Storage Condition Phase W37 canister

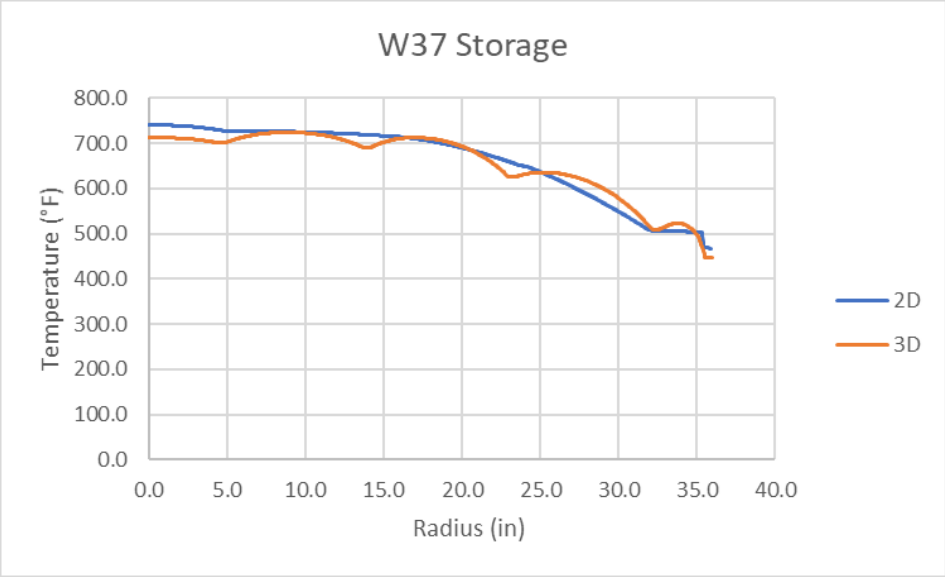

Figure 36 - Temperature Distribution along Radius from the 2D and 3D Results. Storage Condition Phase W21H canister

(a,c)

[

]

Figure 37 – Axial Temperature Distribution in 3D Models of W37 and W21H Canisters during the Vacuum Phase with ACS

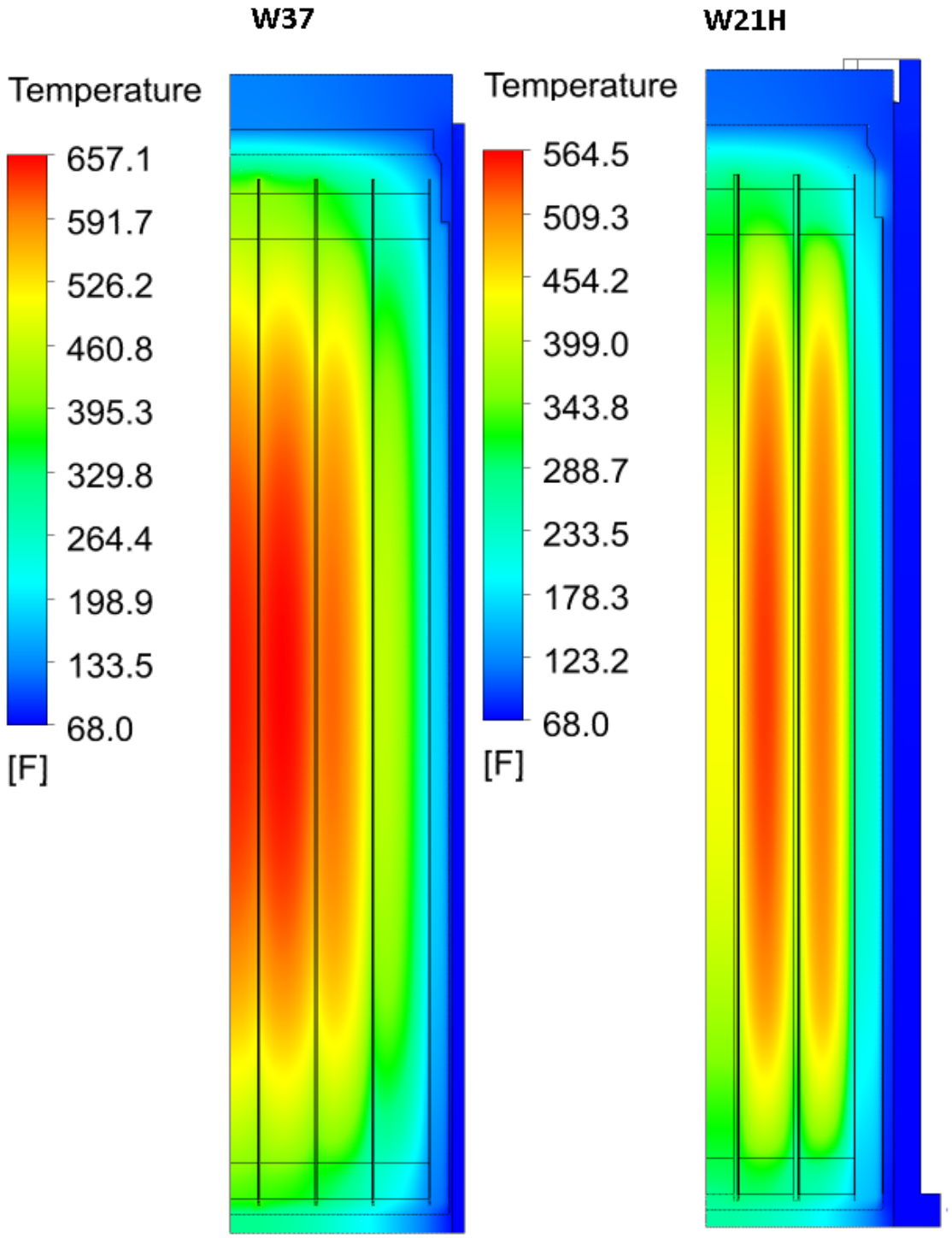

(a,c)

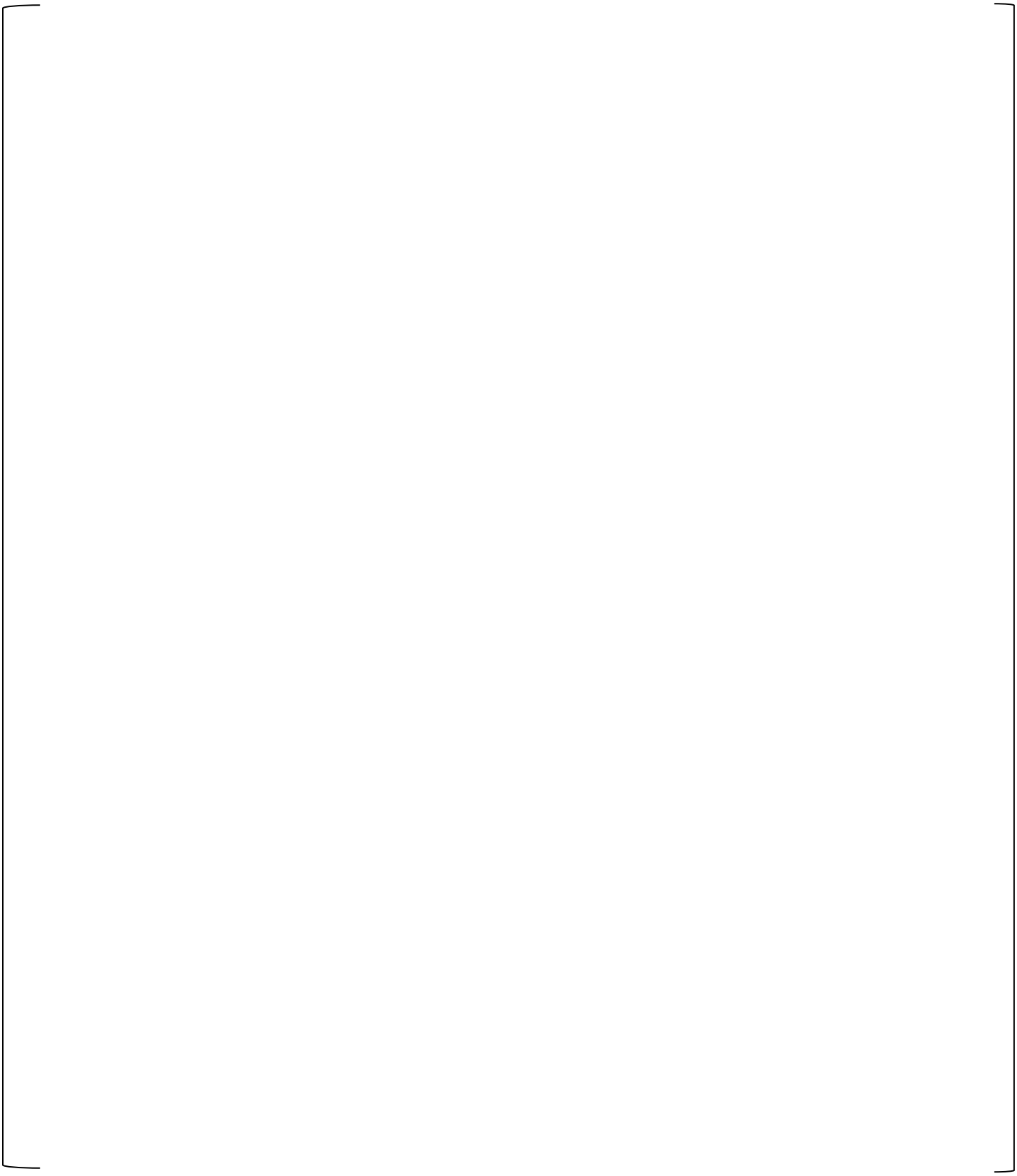

Figure 39 – Axial Temperature Distribution in 3D Models of W37 and W21H Canisters during the Water Phase with ACS

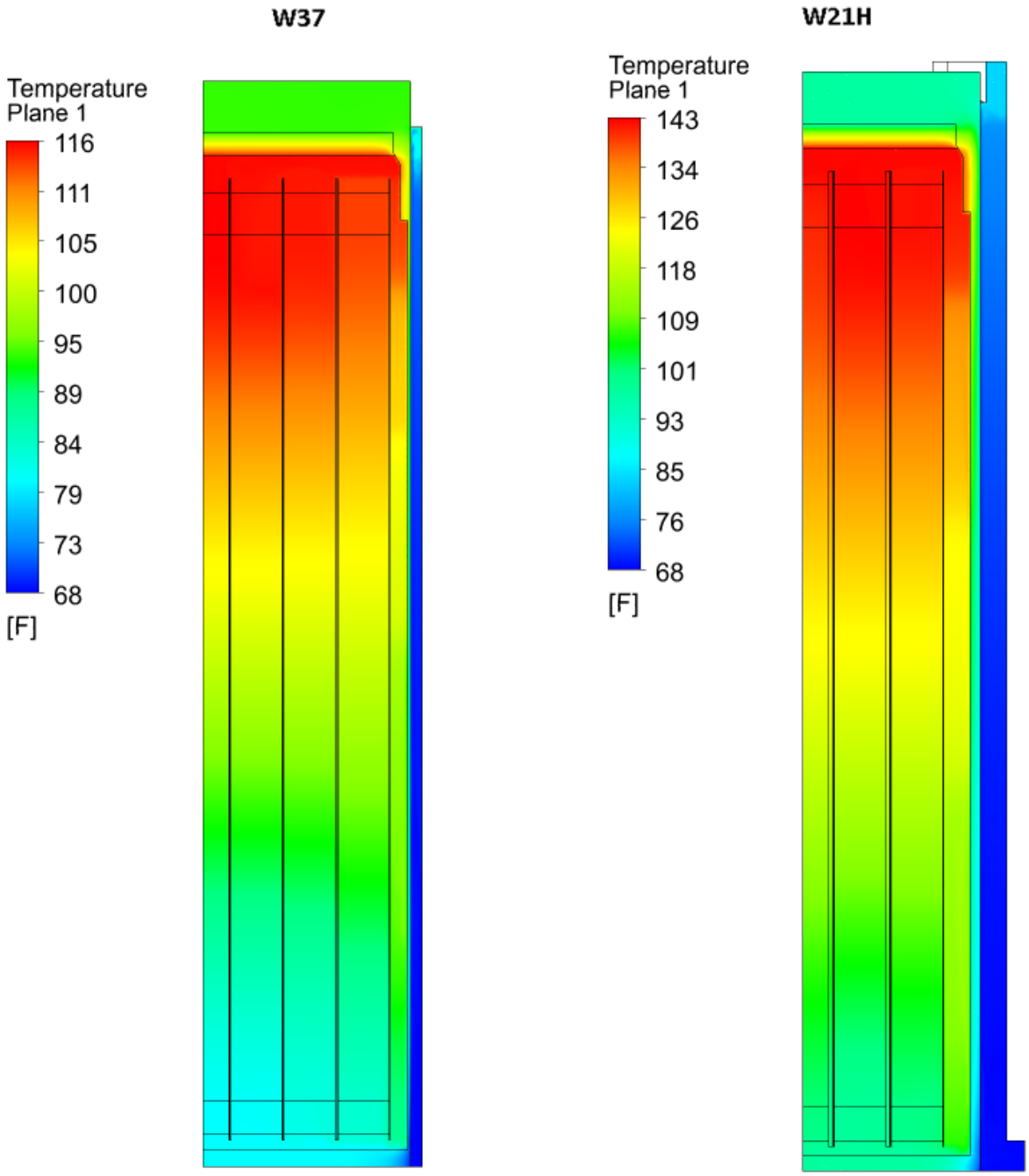

(a,c)

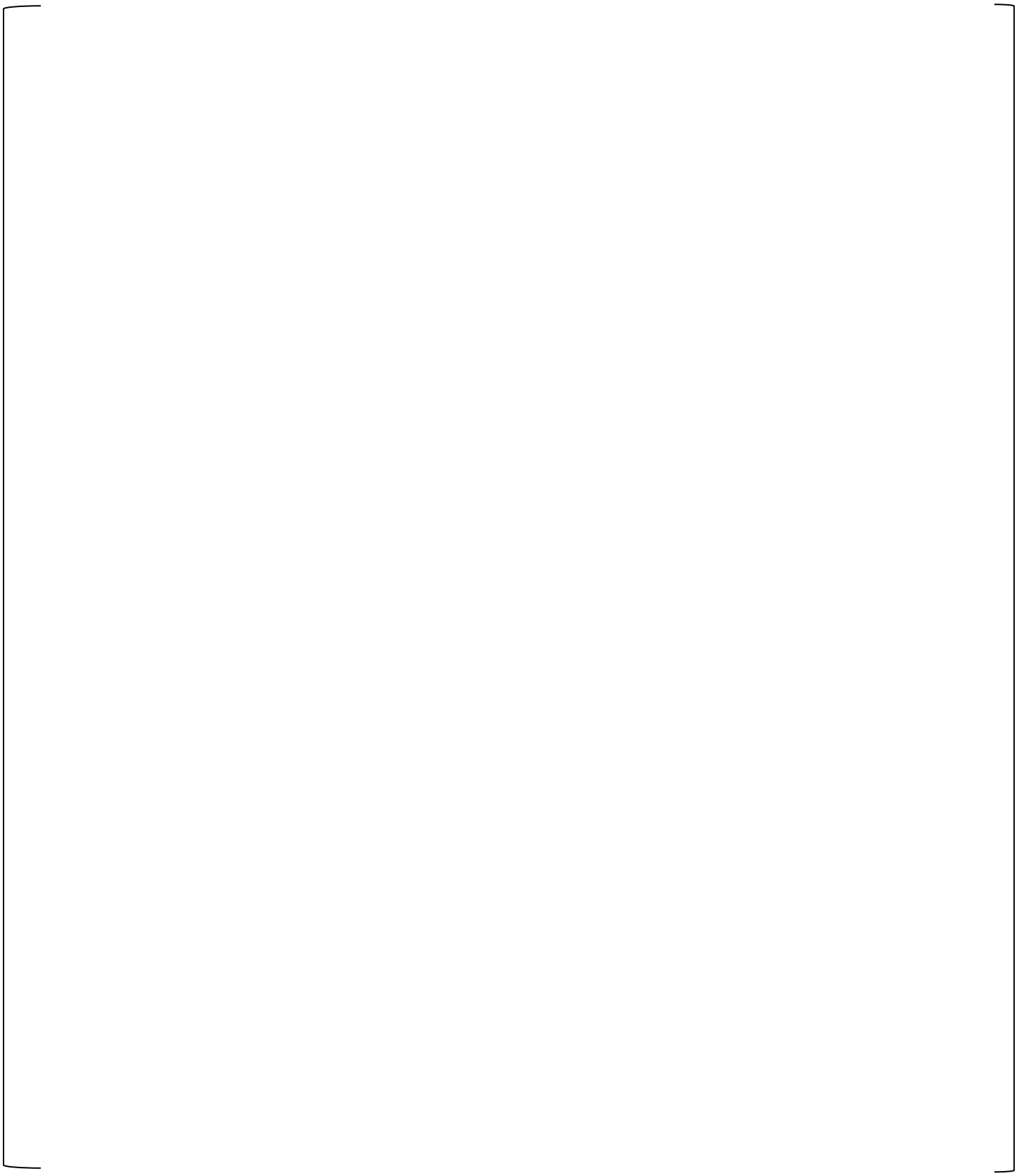

c) In the 3D model, the fins are explicitly modeled (no porous media approximation) in order to correctly represent the heat transfer phenomena in that zone as explained in Section 5.4.1.3.2. In Section 5.4.1.3.1.1, it there is some discussion about the flow field in the space between fins. [

]$^{(a,c)}$

(a,c)

[

]$^{(a,c)}$

(a,c)

(a,c)

(a,c)

[3] The red line show the reduction in temperatures after fins optimization